Ultrafast skyrmion generation by plasmonic resonance

W. Al Saidi, Yannick Dusch, M. Myint, Nicolas Tiercelin, R. Sbiaa

Ultrafast skyrmion generation by plasmonic resonance

W. Al Saidi,[1] Y. Dusch,[2] M. T. Z. Myint,[1] N. Tiercelin,[2] and R. Sbiaa[1,*]

[1]*Department of Physics, College of Science, Sultan Qaboos University, P.O. Box 36, PC 123, Muscat, Oman*

[2]*University of Lille, CNRS, Centrale Lille, Université Polytechnique Hauts-de-France, UMR 8520 - IEMN, 59000 Lille, France*

(Received 16 January 2024; accepted 29 April 2024; published 13 May 2024)

This theoretical study unveils the potential for ultrafast skyrmion generation in magnetic thin films, driven by the remarkable plasmonic properties of gold nanoparticles. By combining the plasmonic, photothermal, and micromagnetic analysis, we explore size-dependent light absorption, resonance wavelength, and electric field distribution around the nanoparticles. Our findings highlight the crucial role of the insulating layer's thickness in enhancing plasmonic effects, offering tunable absorption characteristics. Micromagnetic calculations demonstrate the efficient creation of Néel skyrmions in the range of a few tens of ps, showcasing a breakthrough in magnetic phenomena and opening thus a path for functional skyrmionic-based devices.

DOI: 10.1103/PhysRevB.109.184427

Skyrmions are topologically stable magnetic structures with unique properties, characterized by a swirling spin configuration. These nanoscale quasiparticles have garnered significant attention in recent years for their potential applications in memory, logic, and quantum computing devices [1–7]. Due to their promising applications, the creation of skyrmions has become a focal point in nanomagnetic research. The creation of skyrmions has been realized by several methods, each with its own unique approach. Some skyrmions appear spontaneously due to the dimensions or geometry of the material, while others are formed by the application of electrical currents [8–11], voltage [12], magnetic fields [13–15], spin waves [16], surface acoustic waves [17], laser pulses (local heating) [18,19], and x-ray illumination [20]. However, several limitations still exist in the creation and manipulation of skyrmions, which pose challenges for the development of skyrmion-based technologies. Existing skyrmion creation techniques have drawbacks in terms of energy consumption, scalability, and creation speed. Overcoming these challenges is crucial for realizing the practical applications of skyrmion-based technologies.

In this context, the strong interaction of metal nanoparticles (NPs) with the incident electromagnetic field allows them to exhibit unique optical properties. This interaction gives rise to the localized surface plasmon resonance effect which depends strongly on the geometrical aspects (shape and size) [21,22] and dielectric properties of the surrounding medium [23]. Small variations in these parameters lead to a shift in the optical properties of these NPs and the resulting resonance wavelength can span from the visible to the infrared region (IR).

In this paper, a different approach for ultrafast skyrmions creation by the plasmonic effect generated by gold NPs is proposed. By using pulsed laser irradiation at resonance wavelength, a well-controlled localized heat can be generated leading thus to skyrmion creation. This approach not only contributes to the fundamental understanding of the plasmonic effect in the skyrmion formation but also paves the way for advancements in the development of next-generation magnetic devices.

Figure 1(a) is a schematic diagram of a hemisphere gold NP deposited on a thin magnetic layer that is itself protected from oxidation by 1-nm-thick Pt and a thin film of SiO_2 as an insulator for favoring plasmonic effect. Below the magnetic layer, a 10-nm-thick Ta buffer layer is necessary for good adhesion and better growth of the Co layer. The 3 nm of the magnetic layer can be substituted by a multilayered structure with the interfacial Dzyaloshinskii-Moriya interaction (DMI) [24,25]. A direct correlation between nanoparticle radius (R_{NP}) and the absorbed light can be seen with a greater light absorption achieved from larger NPs as a result of their larger absorption cross sections. The absorption spectra exhibit a peak at the resonance wavelength λ_R at which the NP absorbs light most efficiently. By plotting the resonance wavelength versus the NP radius, a perfect linear dependence can be found as shown in Fig. 1(b). Smaller NPs typically have resonance wavelengths in the visible spectrum, while larger NPs have resonance wavelengths in the near-infrared range. Moreover, this observation aligns with the classical Mie theory, which predicts a linear relationship between the resonance wavelength and the diameter of spherical NPs [26] where in our case we have a hemisphere. We purposefully chose a gold nanoparticle radius of at least 10 nm radius to avoid the significant impact of quantum effects. At this scale, the behavior of particles is governed by classical physics, which supersedes concepts like quantum tunneling and wave-particle duality [27]. The cross-sectional view in Fig. 1(c) illustrates the distribution of the electric field surrounding the nanoparticle with a radius of 15 nm at its plasmonic resonance wavelength. The incident electromagnetic wave excites the conduction electrons in the metal nanoparticle, resulting in a significant enhancement of the electric field. Notably, the maximum electric field is observed at the side of the hemisphere revealing regions with the highest intensity called "hotspots" where the electromagnetic field is concentrated. This enhancement is six orders of magnitude higher than the

*rachid@squ.edu.om

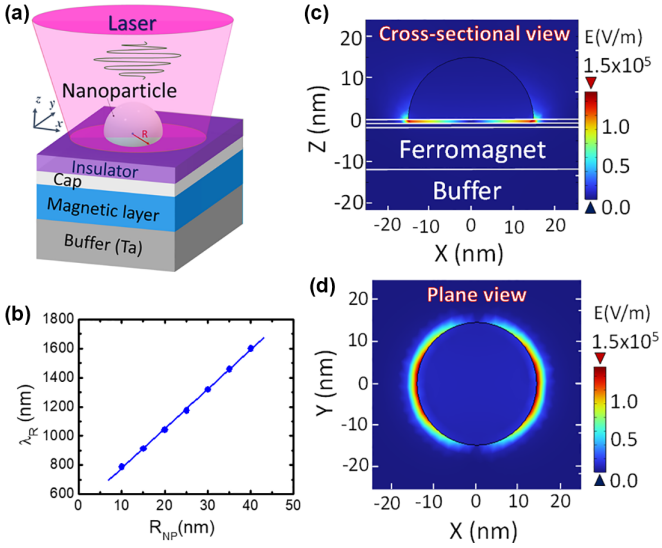

FIG. 1. (a) Schematic representation of hemisphere gold nanoparticle (NP) on top of multilayered thin film. (b) The resonance wavelength as a function of NP radius. Panels (c) and (d) are the cross-sectional and plane views of the electric field distribution for an illuminating wavelength of 915 nm and NP radius of 15 nm, respectively.

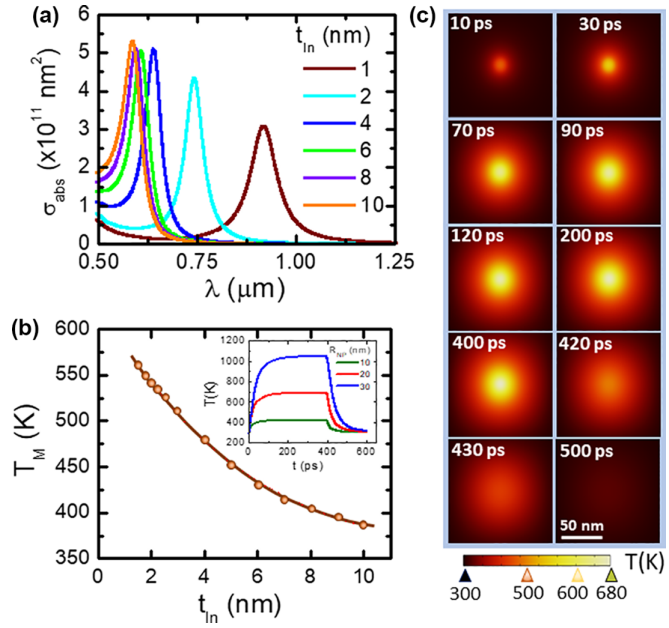

FIG. 2. (a) Absorption spectra of the gold nanoparticle for different insulating layer thicknesses. (b) Maximum temperature on Co layer as a function of insulator thickness, inset graph the evolution of temperature as a function of the irradiation time for different NP sizes with insulator thickness of 1 nm at a laser pulse duration of 400 ps. (c) Calculated temperature profile generated by 20-nm-radius nanoparticle using a laser with an optimal wavelength of 1045 nm, maximizing the surface absorption at 1 nm SiO_2.

incident field strength, compared to the surrounding areas. In the far-field region, the field strength decreases rapidly. The plane view in Fig. 1(d) provides a surface map of the electric field distribution in the plane above the insulating layer. The concentration of the electric field is not uniform across the plane but is instead localized at the sides of the surface. The presence of an insulator layer below NP enhances the plasmonic effects leading to a strong localization of the electric field near the metal-insulator interface. The dielectric layer serves as a waveguide, facilitating the guidance and concentration of light around NP and also serves as a protective shield around it. To further optimize the plasmonic effect, we varied the thickness of the insulating layer while R_{NP} was fixed to 15 nm. The absorption cross section σ_{abs} of different thicknesses is presented in Fig. 2(a). Varying the thickness of the insulator layer has a notable impact on the absorption cross section, particularly on the resonance wavelength. As the insulator layer thickness increases, the resonance wavelength typically experiences a shift toward shorter wavelengths. This blueshift is due to changes in the plasmonic coupling and interactions between the electric field and the nanoparticle. A stronger electromagnetic coupling between the NPs and the insulator layer causes a longer resonance wavelength [28]. The optimal absorption cross section at specific wavelengths can be achieved by optimizing the insulator layer thickness. This allows the creation of structures with ideal absorption properties based on the requirements of the application.

As gold NP absorbs light at their plasmonic resonance wavelength, part of the incident light energy is converted into thermal energy. The generated thermal energy is transferred to the surrounding environment, impacting the temperature of the medium in which the gold NPs are dispersed including the thin film below it.

The heat-transfer analysis was carried out numerically in the current study and is expressed as

$$\partial T/\partial t + U \cdot \nabla T = k/(\rho C_p)\nabla^2 T + q \qquad (1)$$

where, T, t, and $\boldsymbol{U}$ stand for the temperature, time, and velocity vector, respectively. The thermal conductivity k, density ρ, and heat capacity C_p are selected from Refs. [29,30]. The parameter q is the local heat generated per unit time.

Figure 2(b) illustrates the maximum temperature T_M at the magnetic layer surface. A clear exponential decay of T_M with the thickness of the insulating layer is observed. Although σ_{abs} is high at the surface of the Au nanoparticle, the amount of heat reaching the magnetic layer decreases with thicker SiO_2 layers. Thicker insulator layers act as thermal barriers, limiting the transfer of heat to deeper layers.

The Au hemisphere was excited by a laser pulse with an intensity set to 140 mW/mm [31] for a duration τ of 400 ps. It is worth noting that the value of τ is more than required for creating skyrmions as will be discussed in Fig. 4, which is another key advantage of the proposed method for skyrmions formation. Figure 2(b) inset graph shows the temperature generated for three different sizes of NPs with radius of 10, 20, and 30 nm at λ_R of 790, 1045, and 1320 nm, respectively. The absorption is maximized, leading to enhanced absorption of incident light and efficient conversion into heat. The results show that the amount of heat generated increases with the size of NP. Smaller NPs exhibit faster heating and cooling due to their higher surface area-to-volume ratio, whereas larger nanoparticles have slower thermal responses. The results indicate that the photothermal properties of gold NP are size

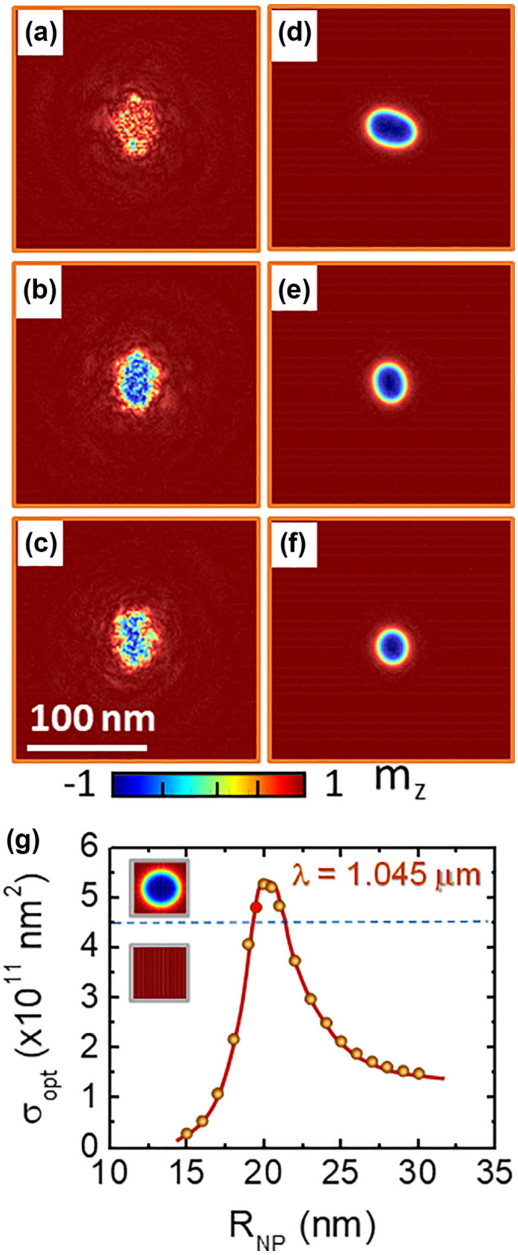

FIG. 3. (a)–(d) Evolution of the skyrmion formation at (a) 100 ps, (b) 200 ps, (c) 300 ps, (d) 500 ps, (e) 700 ps, and (f) 900 ps. (g) Optimal at wavelength of 1045 nm for different gold nanoparticle sizes. The color scale denotes the z component of the spins.

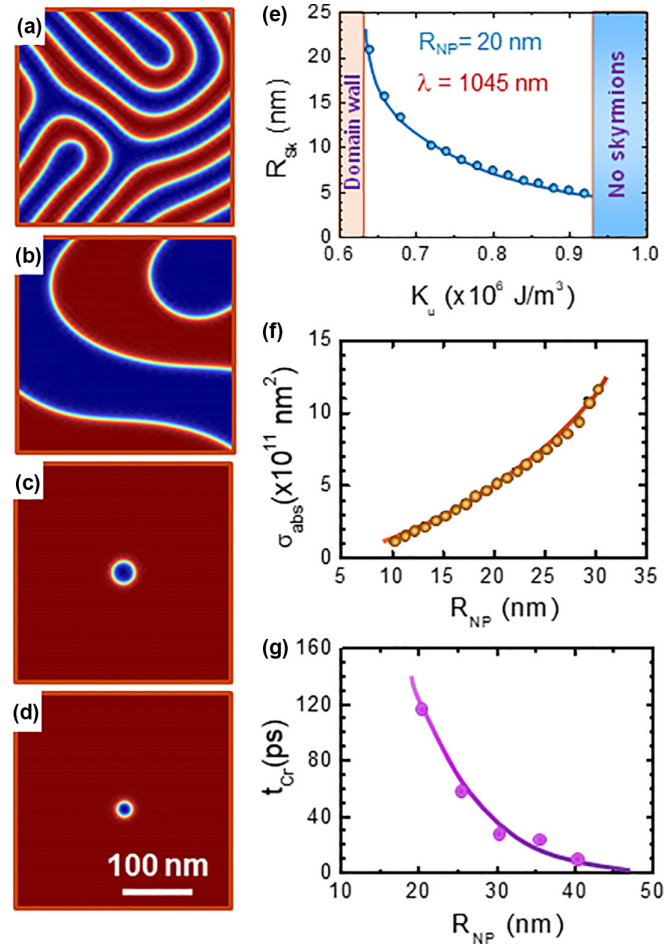

FIG. 4. (a)–(d) Snapshots of magnetization profile showing plasmonic effect on a 20-nm-radius gold nanoparticle for K_u of 0.55, 0.60, 0.65, and 0.70 MJ/m³, respectively. (e) Relationship between skyrmion radius and uniaxial anisotropy constant. (f) Absorption cross section as a function of gold NP radius. (g) Creation time of skyrmion versus gold NP radius.

tunable. The nanoparticle absorbs parts of the incident laser to heat up and this leads to a temperature increase in the surrounding medium. The highest temperature is observed near the surface of the nanoparticle as can be seen in snapshots of Fig. 2(c), captured at the magnetic layer under the conditions of $R_{NP} = 15$ nm, insulator thickness of 1 nm, and λ_R of 915 nm. The localized heating from the nanoparticle at its resonance wavelength serves as a key initiator for the formation of skyrmions.

In the third part of this study, the dynamical behavior of the magnetic moments under plasmonic resonance is investigated using Landau-Lifshitz-Gilbert (LLG) formalism [32]. Illuminating the gold NP at its plasmonic resonance conditions can give rise to various effects, including the generation of heat, electric current, and the production of a magnetic field. Although the values of the magnetic field and electric current were relatively small, their inclusion in the simulation is crucial for a comprehensive understanding of the system's behavior. For an optimal plasmonic effect at a selected nanoparticle of 20 nm, the maximum temperature T_M could reach ~690 K. We selected a common magnetic material such as Ta/Co/Pt [33,34], W/Co/Pt [34,35], Pt/Co/Ir [36,37] with a saturation magnetization M_S of 600 kA/m, exchange stiffness constant A_{ex} of 7.0 pJ/m, DMI strength of 2.0 mJ/m², and damping constant α of 0.1. The uniaxial anisotropy constant K_u was varied between 0.5 and 0.7 MJ/m^3 as it is the most sensitive parameter to the layers interfacing the magnetic layer. The magnetic moments experience random thermal fluctuations during the application of heat generated by the photothermal process from gold NP. As the temperature decreases, the system undergoes phase transitions and the skyrmion emerges in its stable state. Figures 3(a)–3(f) provide snapshots of the formation of a Néel skyrmion with time at K_u of 0.67 MJ/m^3. The visualization captures a specific

moment in the dynamic process, offering insights into the structure and arrangement of the skyrmion. The skyrmion with a diameter of 27 nm is stabilized. To further enhance the understanding, the temporal evolution of the magnetic states is shown in the Supplemental Material [38]. The photothermal effect induced by the gold NP can generate heat at different wavelengths, with a particular focus on the enhanced effect when shining light on the plasmonic resonance wavelength of the gold NP. Our investigation aimed to assess the efficiency of creating skyrmions under selected conditions. We studied different size ranges (R_{NP} between 15 and 30 nm) and specifically calculated the absorption at 1045 nm, corresponding to the resonance wavelength of the 20-nm radius. The methodology involved extracting the temperature profile on the Co layer and implementing it into the LLG equation. The results revealed that the creation of skyrmions was notably effective when R_{NP} was set between 20 and 21 nm, while no skyrmion formation occurred for other radius values as can be seen in Fig. 3(g). This outcome strongly suggests the efficiency of the employed method in generating skyrmions under the specified conditions. This finding underscores the significance of plasmonic resonance at the wavelength of 1045 nm, where the 20-nm radius NPs demonstrated optimal efficiency in inducing the desired photothermal efficiency leading to skyrmion generation. The formation of skyrmion occurs only for $\sigma_{abs} \gtrsim 4.5 \times 10^{11}$ nm^2. The successful generation of skyrmions in this size range highlights the precision and control achievable through the manipulation of NPs properties. Practically, there is a distribution of the size of NPs deposited on the magnetic layer. Skyrmions will be created only from NPs whose sizes match the resonance wavelength. Skyrmions with different sizes can be created by selecting the adequate wavelength.

The stability and characteristics of magnetic textures including skyrmions are influenced by the uniaxial anisotropy constant K_u. In Figs. 4(a)–4(d), the impact of heat on a 20-nm-radius gold nanoparticle is explored for different values of K_u. For K_u of 0.5 MJ/m^3, the plasmonic effect induces the formation of magnetic domains, as illustrated in Fig. 4(a). These domains exhibit remarkable growth with the increase in K_u to 0.6 MJ/m^3, as depicted in Fig. 4(b). For larger K_u values, the creation of the skyrmion was clearly seen [Figs. 4(c) and 4(d)]. This transition within the K_u range reflects a strong interplay between the efficiency of the plasmonic effect and the anisotropy energy in terms of skyrmion creation. In addition to the creation of skyrmion around the nanoparticle, its size can be controlled by adjusting the magnetic anisotropy energy. Figure 4(e) illustrates the relationship between the radius of the created skyrmion and the uniaxial anisotropy. For values below 0.64 MJ/m^3, magnetic domains are produced by the plasmonic effect while skyrmions are created in the range 0.64–0.92 MJ/m^3. The skyrmion radius was found to be exponentially decreasing with K_u. We observed a shrinking of skyrmion from 20 nm to about 5 nm in the investigated conditions. However, beyond 0.92 MJ/m^3, no skyrmion could be created as a result of the existence of a critical size for its stability [39]. The intricate interplay between the plasmonic effect and anisotropy energy provides valuable insights into the tunability of magnetic structures through the manipulation of material parameters. As the size of the skyrmion increases, the time required for its formation becomes longer. This phenomenon can be attributed to the larger size of the skyrmion, which corresponds to a higher σ_{abs}, as can be seen in Fig. 4(f). The larger absorption results in greater heat generation by the plasmonic effect. Another key finding of this study is the ultrafast formation of stable skyrmions by the plasmonic effect. In Fig. 4(e), the relationship between the creation time of the skyrmion and its radius is plotted. It can be observed that the skyrmion creation time *tcr* dropped from 125 ps for a nanoparticle of 20 nm in radius to ∼15 ps for the case of 40 nm radius. This decrease in creation time for larger skyrmions aligns with the trend observed in Fig. 4(f), i.e., larger NPs generate more heat, accelerating the formation of skyrmion.

In conclusion, our study illuminates the promising avenue of ultrafast skyrmion generation through the plasmonic effect from the gold nanoparticle. The precise accuracy achieved by tuning the photothermal properties of the NPs, excitation wavelength, and the exposure time coupled with the interplay of material parameters, opens possibilities for applications in advanced data storage and logic devices. Besides the formation of skyrmions by plasmonic resonance, the time needed for this process could reach less than 20 ps. This leads to a very low energy requirement for ultrafast creation of skyrmions.

The authors would like to thank M. Klaui from Gutenberg University Mainz for valuable discussions. R.S. would like to acknowledge the support from the HMTF Strategic Research of Oman (Grant No. SR/SCI/PHYS/20/01).

R.S. conceived the idea and analyzed the data. W.S. conducted the simulation and interpreted the results. M.M. analyzed the data. Y.D. and N.T. contributed to the interpretation of the results. All authors discussed the results and provided input to the manuscript.

The authors declare no competing interests.

[1] G. Yu, P. Upadhyaya, Q. Shao, H. Wu, G. Yin, X. Li, C. He, W. Jiang, X. Han, P. K. Amiri, and K. L. Wang, Room-temperature skyrmion shift device for memory application, Nano Lett. **17**, 261 (2017).

[2] Y. Jiang, H. Yu, and X. Chen, Skyrmion-based racetrack multilevel data storage device manipulated by pinning, J. Appl. Phys. **134**, 053901 (2023).

[3] W. Koshibae Y. Kaneko, J. Iwasaki, M. Kawasaki, Y. Tokura, and N. Nagaosa, Memory functions of magnetic skyrmions, Jpn. J. Appl. Phys. **54**, 053001 (2015).

[4] N. Sisodia, J. Pelloux-Prayer, L. D. Buda-Prejbeanu, L. Anghel, G. Gaudin, and O. Boulle, Programmable skyrmion logic gates based on skyrmion tunneling, Phys. Rev. Appl. **17**, 064035 (2022).

[5] M. G. Mankalale, Z. Zhao, J.-P. Wang, and S. S. Sapatnekar, SkyLogic—A Proposal for a skyrmion-based logic device, IEEE Trans. Electron Dev. **66**, 1990 (2019).

[6] Z. R. Yan, Y. Z. Liu, Y. Guang, K. Yue, J. F. Feng, R. K. Lake, G. Q. Yu, and X. F. Han, Skyrmion-based programmable logic

device with complete boolean logic functions, Phys. Rev. Appl. **15**, 064004 (2021).
[7] C. Psaroudaki and C. Panagopoulos, Skyrmion qubits: A new class of quantum logic elements based on nanoscale magnetization, Phys. Rev. Lett. **127**, 067201 (2021).
[8] Y. Tchoe and J. H. Han, Skyrmion generation by current, Phys. Rev. B **85**, 174416 (2012).
[9] H. Y. Yuan and X. R. Wang, Skyrmion creation and manipulation by nano-second current pulses, Sci. Rep. **6**, 22638 (2016).
[10] W. Legrand, D. Maccariello, N. Reyren, K. Garcia, C. Moutafis, C. Moreau-Luchaire, S. Collin, K. Bouzehouane, V. Cros, and A. Fert, Room-temperature current-induced generation and motion of sub-100 nm skyrmions, Nano Lett. **17**, 2703 (2017).
[11] W. Al Saidi and R. Sbiaa, Stabilizing magnetic skyrmions on constricted nanowires, Sci. Rep. **12**, 10141 (2022).
[12] R. Ishikawa, M. Goto, H. Nomura, and Y. Suzuki, Controlling the creation/annihilation and distribution of magnetic skyrmions by manipulating an externally applied voltage, Appl. Phys. Lett. **121**, 252402 (2022).
[13] M. Stier, W. Häusler, T. Posske, G. Gurski, and M. Thorwart, Skyrmion–anti-Skyrmion pair creation by in-plane currents, Phys. Rev. Lett. **118**, 267203 (2017).
[14] N. Romming, C. Hanneken, M. Menzel, J. E. Bickel, B. Wolter, K. von Bergmann, A. Kubetzka, and R. Wiesendanger, Writing and deleting single magnetic skyrmions, Science **341**, 636 (2013).
[15] N. Mathur F.S. Yasin, M. J. Stolt, T. Nagai, K. Kimoto, H. Du, M. Tian, Y. Tokura, X. Yu, and S. Jin, In-plane magnetic field-driven creation and annihilation of magnetic skyrmion strings in nanostructures, Adv. Funct. Mater. **31**, 2008521 (2021).
[16] Y. Liu, G. Yin, J. Zang, J. Shi, and K. R. Lake, Skyrmion creation and annihilation by spin waves, Appl. Phys. Lett. **107**, 152411 (2015).
[17] T. Yokouchi, S. Sugimoto, B. Rana, S. Seki, N. Ogawa, S. Kasai, and Y. Otani, Creation of magnetic skyrmions by surface acoustic waves, Nat. Nanotechnol. **15**, 361 (2020).
[18] S. G. Je, P. Vallobra, T. Srivastava, J.-C. Rojas-Sánchez, T. H. Pham, M. Hehn, G. Malinowski, C. Baraduc, S. Auffret, G. Gaudin *et al.*, Creation of magnetic skyrmion bubble lattices by ultrafast laser in ultrathin films, Nano Lett. **18**, 7362 (2018).
[19] K. Gerlinger, B. Pfau, F. Buttner, M. Schneider, L.-M. Kern, J. Fuchs, D. Engel, C. M. Gunther, M. Huang, I. Lemesh *et al.*, Application concepts for ultrafast laser-induced skyrmion creation and annihilation, Appl. Phys. Lett. **118**, 192403 (2021).
[20] Y. Guang, I. Bykova, Y. Liu, G. Yu, E. Goering, M. Weigand, J. Gräfe, S. K. Kim, J. Zhang, H. Zhang *et al.*, Creating zero-field skyrmions in exchange-biased multilayers through X-ray illumination, Nat. Commun. **11**, 949 (2020).
[21] E. Ringe, M. R. Langille, K. Sohn, J. Zhang, J. Huang, C. A. Mirkin, R. P. Van Duyne, and D. L. Marks Plasmon length: A universal parameter to describe size effects in gold nanoparticles, J. Phys. Chem. Lett. **3**, 1479 (2012).
[22] D. E. Mustafa, T. Yang, Z. Xuan, S. Chen, H. Tu, and A. Zhang, Surface plasmon coupling effect of gold nanoparticles with different shape and size on conventional surface plasmon resonance signal, Plasmonics **5**, 221 (2010).
[23] E. A. Chaffin, S. Bhana, R. T. O'Connor, X. Huang, and Y. Wang, Impact of core dielectric properties on the localized surface plasmonic spectra of gold-coated magnetic core–shell nanoparticles, J. Phys. Chem. B **118**, 14076 (2014).
[24] M. Belmeguenai, J.-P. Adam, Y. Roussigné, S. Eimer, T. Devolder, J.-V. Kim, S. M. Cherif, A. Stashkevich, and A. Thiaville, Interfacial Dzyaloshinskii-Moriya interaction in perpendicularly magnetized Pt/Co/AlOx ultrathin films measured by Brillouin light spectroscopy, Phys. Rev. B **91**, 180405(R) (2015).
[25] J.-H. Kim, J.-B. Lee, G.-G. An, S.-M. Yang, W.-S. Chung, H.-S. Park, and J.-P. Hong, Ultrathin W space layer-enabled thermal stability enhancement in a perpendicular MgO/CoFeB/W/CoFeB/MgO recording frame, Sci. Rep. **5**, 16903 (2015).
[26] E. G. Wrigglesworth and J. H. Johnston, Mie theory and the dichroic effect for spherical gold nanoparticles: An experimental approach, Nanoscale Adv. **3**, 3530 (2021).
[27] U. Kreibig and M. Vollmer, *Optical Properties of Metal Clusters*, Springer Series in Materials Science, Vol. 25 (Springer, New York, 2013).
[28] J. Son, Y. Lee, J. H. Ahn, and H. Yang, Shifting of surface plasmon resonance due to electromagnetic coupling between graphene and Au nanoparticles, Opt. Express **20**, 19690 (2012).
[29] Y. A. Cengel and A. J. Ghajar, *Heat and Mass Transfer: Fundamentals and Applications*, 5th ed. (McGraw-Hill New York, 2020).
[30] R. Borah, A. Kumar, M. Samantaray, A. Desai, and F.-G. Tseng, Photothermal heating of Au nanorods and nanospheres: Temperature characteristics and strength of convective forces, Plasmonics **18**, 1449 (2023).
[31] Y. Kikuchi and T. Tanaka, Strengthen of magnetic anisotropy of Au/Co/Au nanostructure by surface plasmon resonance, Sci. Rep. **9**, 8630 (2019).
[32] A. Vansteenkiste, J. Leliaert, M. Dvornik, M. Helsen, F. Garcia-Sanchez, and B. Van Waeyenberge, The design and verification of MuMax3, AIP Adv. **4**, 107133 (2014).
[33] S. Woo, M. Mann, A. J. Tan, L. Caretta, and S. D. G. Beach, Enhanced spin-orbit torques in Pt/Co/Ta heterostructures, Appl. Phys. Lett. **105**, 212404 (2014).
[34] X. Wang, A. Cao, S. Li, J. Tang, A. Du, H. Cheng, Y. Sun, H. Du, X. Zhang, and W. Zhao, Manipulating density of magnetic skyrmions via multilayer repetition and thermal annealing, Phys. Rev. B **104**, 064421 (2021).
[35] S. K. Jena, R. Islam, E. Milińska, M. M. Jakubowski, R. Minikayev, S. Lewińska, A. Lynnyk, A. Pietruczik, P. Aleszkiewicz, C. Autieri *et al.*, Interfacial Dzyaloshinskii–Moriya interaction in the epitaxial W/Co/Pt multilayers, Nanoscale **13**, 7685 (2021).
[36] M. Baćani, M. A. Marioni, J. Schwenk, and H. J. Hug, How to measure the local Dzyaloshinskii-Moriya interaction in skyrmion thin-film multilayers, Sci. Rep. **9**, 3114 (2019).
[37] M. Cubukcu, S. Pöllath, S. Tacchi, A. Stacey, E. Darwin, C. W. F. Freeman, C. Barton, B. J. Hickey, C. H. Marrows, G. Carlotti *et al.* Manipulation of magnetic skyrmion density in continuous Ir/Co/Pt multilayers, Micromachines **13**, 1911 (2022).
[38] See Supplemental Material at http://link.aps.org/supplemental/10.1103/PhysRevB.109.184427 for the formation of a skyrmion by plasmonic effect.
[39] W. Al Saidi, R. Sbiaa, S. Bhatti, S. N. Piramanayagam, and S. Al Risi, Dynamics of interacting skyrmions in magnetic nanotrack, J. Phys. D: Appl. Phys. **56**, 355001 (2023).